



AFRL-RX-TY-TR-2012-0046

SELF-COOLING GRADIENT SHELL FOR BODY ARMOR

Igor Luzinov, Konstantin G. Komev

School of Materials Science and Engineering
Clemson University
161 Surrine Hall
Clemson, SC 29634

Contract No. FA8650-09-D-5900-0003

May 2012

DISTRIBUTION A: Approved for public release; distribution unlimited.
88ABW-2012-5358, 10 October 2012.

**AIR FORCE RESEARCH LABORATORY
MATERIALS AND MANUFACTURING DIRECTORATE**

DISCLAIMER

Reference herein to any specific commercial product, process, or service by trade name, trademark, manufacturer, or otherwise does not constitute or imply its endorsement, recommendation, or approval by the United States Air Force. The views and opinions of authors expressed herein do not necessarily state or reflect those of the United States Air Force.

This report was prepared as an account of work sponsored by the United States Air Force. Neither the United States Air Force, nor any of its employees, makes any warranty, expressed or implied, or assumes any legal liability or responsibility for the accuracy, completeness, or usefulness of any information, apparatus, product, or process disclosed, or represents that its use would not infringe privately owned rights.

NOTICE AND SIGNATURE PAGE

Using Government drawings, specifications, or other data included in this document for any purpose other than Government procurement does not in any way obligate the U.S. Government. The fact that the Government formulated or supplied the drawings, specifications, or other data does not license the holder or any other person or corporation; or convey any rights or permission to manufacture, use, or sell any patented invention that may relate to them.

This report was cleared for public release by the 88th Air Base Wing Public Affairs Office at Wright Patterson Air Force Base, Ohio available to the general public, including foreign nationals. Copies may be obtained from the Defense Technical Information Center (DTIC) (<http://www.dtic.mil>).

AFRL-RX-TY-TR-2012-0046 HAS BEEN REVIEWED AND IS APPROVED FOR PUBLICATION IN ACCORDANCE WITH ASSIGNED DISTRIBUTION STATEMENT.

OWENS.JEFFERY.
RAY.1235753983

Digitally signed by
OWENS.JEFFERY.RAY.1235753983
DN: c=US, o=U.S. Government, ou=DoD, ou=PKI,
ou=USAF, cn=OWENS.JEFFERY.RAY.1235753983
Date: 2012.10.02 14:29:52 -0500

JEFFERY R. OWENS, PhD
Work Unit Manager

HENLEY.MICHAEL
L.V.1231823332

Digitally signed by HENLEY.MICHAEL.V.1231823332
DN: c=US, o=U.S. Government, ou=DoD, ou=PKI,
ou=USAF, cn=HENLEY.MICHAEL.V.1231823332
Date: 2012.10.01 15:02:33 -0500

MICHAEL V. HENLEY
Chief, Airbase Sciences Branch

RHODES.ALBERT
.N.III.1175488622

Digitally signed by
RHODES.ALBERT.N.III.1175488622
DN: c=US, o=U.S. Government, ou=DoD, ou=PKI,
ou=USAF, cn=RHODES.ALBERT.N.III.1175488622
Date: 2012.10.03 10:10:49 -0500

ALBERT N. RHODES, PhD
Chief, Airbase Technologies Division

This report is published in the interest of scientific and technical information exchange, and its publication does not constitute the Government's approval or disapproval of its ideas or findings.

REPORT DOCUMENTATION PAGE

*Form Approved
OMB No. 0704-0188*

The public reporting burden for this collection of information is estimated to average 1 hour per response, including the time for reviewing instructions, searching existing data sources, gathering and maintaining the data needed, and completing and reviewing the collection of information. Send comments regarding this burden estimate or any other aspect of this collection of information, including suggestions for reducing the burden, to Department of Defense, Washington Headquarters Services, Directorate for Information Operations and Reports (0704-0188), 1215 Jefferson Davis Highway, Suite 1204, Arlington, VA 22202-4302. Respondents should be aware that notwithstanding any other provision of law, no person shall be subject to any penalty for failing to comply with a collection of information if it does not display a currently valid OMB control number.

PLEASE DO NOT RETURN YOUR FORM TO THE ABOVE ADDRESS.

1. REPORT DATE (DD-MM-YYYY) 10-MAY-2012	2. REPORT TYPE Final Technical Report	3. DATES COVERED (From - To) 07-OCT-2010 -- 16-APR-2012
---	---	---

4. TITLE AND SUBTITLE Self-Cooling Gradient Shell for Body Armor	5a. CONTRACT NUMBER FA8650-09-D-5900-0003
	5b. GRANT NUMBER
	5c. PROGRAM ELEMENT NUMBER 0909999F

6. AUTHOR(S) Luzinov, Igor; Komev, Konstantin G.	5d. PROJECT NUMBER GOVT
	5e. TASK NUMBER L0
	5f. WORK UNIT NUMBER X090 (QL102023)

7. PERFORMING ORGANIZATION NAME(S) AND ADDRESS(ES) School of Materials Science and Engineering Clemson University 161 Serrine Hall Clemson, SC 29634	8. PERFORMING ORGANIZATION REPORT NUMBER
---	---

9. SPONSORING/MONITORING AGENCY NAME(S) AND ADDRESS(ES) Air Force Research Laboratory Materials and Manufacturing Directorate Airbase Technologies Division 139 Barnes Drive, Suite 2 Tyndall Air Force Base, FL 32403-5323	10. SPONSOR/MONITOR'S ACRONYM(S) AFRL/RXQL
	11. SPONSOR/MONITOR'S REPORT NUMBER(S) AFRL-RX-TY-TR-2012-0046

12. DISTRIBUTION/AVAILABILITY STATEMENT
Distribution A: Approved for public release; distribution unlimited.

13. SUPPLEMENTARY NOTES
Ref Public Affairs Case # 88ABW-2012-5358, 10 October 2012. Document contains color images.

14. ABSTRACT
Current methods of reducing physiological strain on a soldier wearing armor vest need significant improvement. To this end, the major objective of this work was to conduct research on development of effective lightweight evaporative cooling system capable of delivering significant cooling effect without or with minimal power requirements and additional weight load. During the project we developed major methodology and equipment to measure cooling power and temperature effect of virtually any cooling system arrangements in laboratory conditions reliably. Resultantly, Surface Differential Scanning Calorimeter (SDSC) was created. In addition, we design and test a novel autonomous evaporative cooling system. As a result of the work several cooling arrangements utilizing an evaporative cooling mechanism were created. The driving force enabling significant evaporation is the temperature difference between parts of the arrangement created by cooling metal foil located on the outside of the vest. The best system demonstrated cooling power of about 100 W/m² and surface cooling effect of 7-8 °C without using any external power source. The system is extremely lightweight, compact and self-sufficient. We also developed the procedure for preparation of hydrophobic membrane assembly and large hydrophobic-hydrophilic gradient fabric for directional water transport inside of the cooling system.

15. SUBJECT TERMS
thermal burden, SDSC, cooling, evaporative, textile

16. SECURITY CLASSIFICATION OF:			17. LIMITATION OF ABSTRACT UU	18. NUMBER OF PAGES 24	19a. NAME OF RESPONSIBLE PERSON Jeffery R. Owens
a. REPORT U	b. ABSTRACT U	c. THIS PAGE U			19b. TELEPHONE NUMBER (Include area code)

TABLE OF CONTENTS

LIST OF FIGURES	ii
LIST OF TABLES	ii
1. SUMMARY	1
2. INTRODUCTION	2
3. METHODS, ASSUMPTIONS, AND PROCEDURES	3
3.1. Surface Differential Scanning Calorimeter (SDSC)	3
3.2. Membrane Assembly	5
3.3. Gradient Fabric	6
4. RESULTS AND DISCUSSIONS	7
4.1. Membrane Assembly	7
4.2. Surface Differential Scanning Calorimeter (SDSC)	9
4.3. Initial Experiments	10
4.3.1. Single-Membrane and Membrane Assembly	10
4.3.2. Influence of Air Gap and Water Absorbents	11
4.4. Gradient Fabric	12
4.5. Cooling Systems	13
4.5.1. Small Samples (10 cm × 10 cm)	13
4.5.2. Large Samples (20-cm × 20-cm)	17
4.6. Ultimate Design of the Cooling System	18
5. CONCLUSIONS	19
6. REFERENCES	20
LIST OF SYMBOLS, ABBREVIATIONS, AND ACRONYMS	22

LIST OF FIGURES

	Page
Figure 1. Schematic Drawing of the SDSC Experimental Setup.....	3
Figure 2. Reference (left) and Sample System (right) Arrangements Showing (a) the Styrofoam Insulation, (b, c) the Cotton Wicking Layer, (d) the Water Reservoir, and (e) the Test Sample	4
Figure 3. Controlled-Temperature-and-Humidity Chamber.....	4
Figure 4. Sample of the Membrane Assembly: Flat (left) and Bent (right).....	7
Figure 5. Membrane Assembly Made with 90- μm (top) and 330- μm (bottom) Wires	7
Figure 6. AFM Images of the Membrane: Original (left) and Modified with PGMA (right)	7
Figure 7. Water Droplets on Membranes Treated with a) Lauric Acid and b) Perfluorododecanoic Acid	8
Figure 8. Water Condensation inside the Membrane Assembly.....	9
Figure 9. Power Supplied to Identical Reference and Sample Systems at Different Set Temperatures.....	9
Figure 10. Experimental Results for the Set-up: without Top Insulation with Bare Fabric and the Fabric Covered with the Membrane (left); with Top Insulation and the Membrane Assembly on Top of the Fabric (right)	10
Figure 11. Experimental Results for Power (left) and Temperature Difference (right) for Various Size of Air Gap between the Fabric and the Top Insulation	11
Figure 12. Water Condensed on the Top Insulation's Surface Facing the Fabric	11
Figure 13. Water Droplets and Contact Angles on Fabrics Modified with PGMA (130°) (left); PS-COOH (140°) (middle) and PAA (Completely Wetted) (right)	12
Figure 14. Cooling Power (left) and Temperature Effect (right).....	14
Figure 15. Schematic Representation of Cooling Systems: Standard (top left); with Bare Metal Foil at the Top (top right); with the Foil Covered with Wet Fabric at the Top (bottom left); and System III Isolated from the Outside Environment (bottom right)	14
Figure 16. Cooling Power (left) and Temperature Effect (right) of the Standard Cooling Arrangement (System I) with Modified Fabrics and System II (Aluminum Foil)	15
Figure 17. Cooling Power Measured for Cooling System Arrangements I–IV.....	15
Figure 18. Cooling Power for System III in Presence of Gradient and PAA Fabrics	16
Figure 19. Improved Cooling Arrangement—System V (top) and Cooling Power Produced by System V (bottom).....	17
Figure 20. Cooling Power (left) and Temperature Effect (right) of System V Using the Larger Heater	18
Figure 21. Schematic Representation of the Ultimate Design of the Cooling System.....	18

LIST OF TABLES

	Page
Table 1. Results of Evaporation Tests	8
Table 2. Results of the Experiments Aimed to Eliminate the Condensate	12
Table 3. Contact Angle Values Along the Gradient Fabric Length.....	13

1. SUMMARY

Current methods of reducing physiological stress on a soldier wearing an armor vest need significant improvement. To this end, the major objective of this work was to develop an effective lightweight evaporative cooling system capable of delivering a significant amount of cooling without or with minimal power consumption and added weight. During the project we developed major methodology and equipment to measure cooling power and the thermal effect of virtually any cooling system arrangement reliably, in laboratory conditions. As a result, the surface differential scanning calorimeter (SDSC) was created. In addition, we designed and tested a novel, autonomous system that operates by evaporative cooling. During this contract, several cooling arrangements utilizing an evaporative cooling mechanism were created. The driving force enabling significant evaporation was the temperature difference between parts of the devices, created by a cooling metal foil located on the outside of the vest. The best system demonstrated cooling power of about 100 Wm^{-2} and surface cooling of 7–8 °C without using an external power source. The system is extremely lightweight, compact and self-sufficient. We also developed a procedure for preparation of hydrophobic membrane assemblies and a fabric featuring a large hydrophobic–hydrophilic gradient to drive directional water transport inside the cooling system.

2. INTRODUCTION

Materials for protective clothing have a high fiber density that significantly decreases their permeability. A reduction of the material's permeability results in a dramatic decrease of the natural efficiency of evaporative cooling of the human body and, in many cases, it leads to thermal stresses [1, 2]. Design of materials with efficient heat transport characteristics requires a reliable instrument that would be able to evaluate the materials performance at different environmental conditions. Quantitative analysis of thermodynamic and heat transfer properties of thin fibrous and porous materials is a challenging task. In this report, we demonstrate an instrument that allows one to evaluate the heat transfer properties of different fabrics.

There are three major approaches to measure the fabric performance. The first method is based on the analysis of physiological data (skin temperature, heart rate, etc.) during various types of physical activities performed by humans. The majority of all available published papers on the subject of cooling utilize this method [3–9]. The second approach is evaluation of the system using a guarded sweating hot plate [10]. It is designed to determine the thermal and evaporative resistance of materials producing numerical values for both temperature and power gains in cooling systems. While this approach delivers reliable results, the high cost of the plate does not allow its widespread utilization in laboratory conditions. The third approach uses a thermal manikin and can be described as an advantageous combination of the former two approaches, with both temperature and heat values accessible [11–14]. However the apparent attractiveness of the last approach is diminished by the high expenses associated with the purchasing of the manikin. This method/apparatus was used to demonstrate the cooling capacity of novel smart textile materials for advanced, light-weight, self-cooling protective clothing. Passive cooling was accomplished by creating a laminated structure with a prescribed permeability gradient and electrodes to accelerate moisture transport within the system.

3. METHODS, ASSUMPTIONS AND PROCEDURES

3.1. Surface Differential Scanning Calorimeter (SDSC)

The SDSC consists of a computer, a data acquisition system (Keithley 2700), two power supplies (TDK-Lambda ZUP) to heat thin/flexible Kapton heaters with low lateral heat loss (Omega Engineering, Inc.), and resistance temperature detector (RTD) sensors (Omega Engineering, Inc.) placed at the center and a corner of the heaters. The computer runs a LabView program implementing a proportional integral (PI) control algorithm and a data logging algorithm (Figure 1).

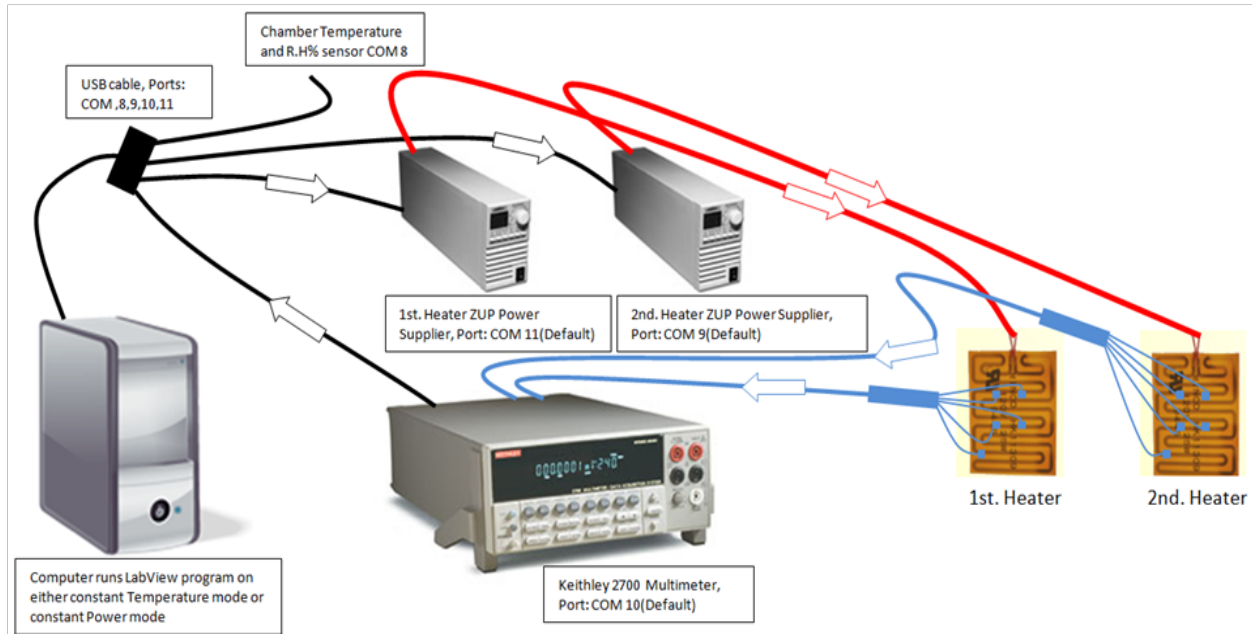


Figure 1. Schematic Drawing of the SDSC Experimental Setup

The design of the system is based on the standard test method for thermal and evaporative resistance of clothing materials using a sweating hot plate (ASTM F1868). As shown in Figure 2, the SDSC has two heating systems. Thin, flexible 10-cm × 10-cm Kapton heating films (Figure 2 (right)) are placed onto the Styrofoam insulation (b). Thus, heat flows only upward. The heaters in both systems are covered entirely by cotton fabrics (Figure 2c). Cotton fabrics are dipped into water (Figure 2d) to keep them wet, thus, simulating a body surface. Materials under testing (Figure 2e) are positioned between the fabric and the top insulation.

The first system—the reference system—is isolated from the ambient environment by covering the fabric’s surface with a plastic film and Styrofoam insulation (simulating impermeable clothing). This prevents evaporation and gives the temperature and power values for a non-evaporating condition. The second—sample—system is used to test the evaporative heat transfer of the cooling arrangement of interest and incorporates top Styrofoam insulation (“the clothing”).

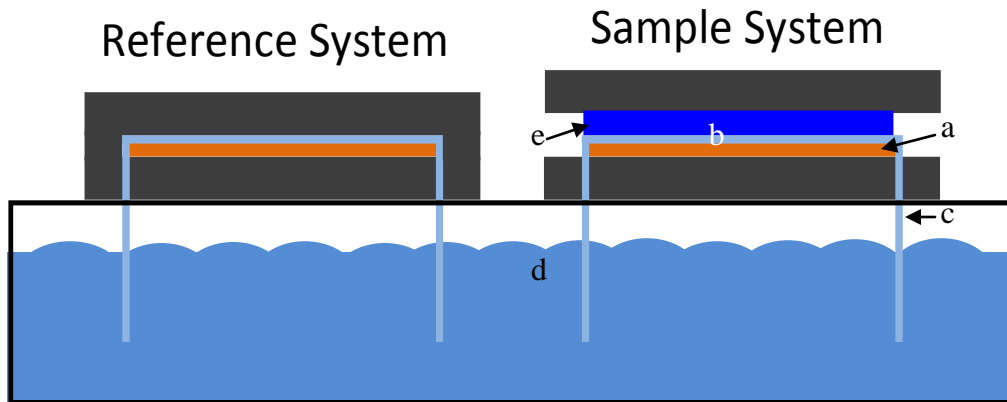


Figure 2. Reference (left) and Sample System (right) Arrangements Showing (a) the Styrofoam Insulation, (b, c) the Cotton Wicking Layer, (d) the Water Reservoir, and (e) the Test Sample

The SDSC operates in two modes, constant power and constant temperature. In constant-power mode, the same power is supplied to both systems while temperatures of the two heating films are monitored. The temperature difference is a value characteristic of the evaporative efficiency of the arrangement. In constant-temperature mode, the systems are maintained at the same constant temperature and the power supplied to each system is monitored. The increase in power required to hold the sample heating system at the same temperature is another value characteristic of the efficiency of the sample's evaporative cooling.

To carry out actual experiments, the SDSC was placed in a controlled-temperature-and-humidity chamber (Thermal Product Solutions) (Figure 3). Variations in temperature and RH inside the chamber were ± 0.5 °C and ± 2 %, respectively, and synchronous, whence we can state that the absolute concentration of water vapor in the chamber stayed constant and only the temperature changed. All experiments were run at 35 °C and variable RH inside the chamber. In temperature-



Figure 3. Controlled-Temperature-and-Humidity Chamber

controlled mode the temperature of all heaters was set to 40 °C. In power-controlled mode the power supplied to the heaters was adjusted to hold a temperature of 40 °C in the reference system. The detailed experimental procedure was as follows: desired conditions inside the chamber were reached (equilibrated in ~ 1 h); temperature control mode was executed (the system equilibrated in ~ 1 h); then power-control mode was executed (the system reequilibrated in ~ 1 h).

Various cooling arrangements were tested. For all systems tested plastic spacers of appropriate height were used to separate top and bottom insulation. The surface of the top insulation facing the heater in the sample system was covered with plastic film to prevent the transport of water vapor through the insulation. The abovementioned arrangement was used when influence of air gap and evaporation through the membrane or membrane assembly were studied.

In the experiments using a metal foil (copper (Cu) or aluminum (Al)) the foil itself was attached to the top insulation. The cooling systems are described in more detail in the Results and Discussions section.

3.2. Membrane Assembly

Materials used:

- Poly(glycidyl methacrylate) (PGMA) ($M_n = 300,000$ Da, PDI = 2);
- Lauric and perfluorododecanoic acids;
- Poly(ethylene terephthalate) membrane (Sterlitech Corp., pore size = 400 nm, thickness = 10 μm , calculated porosity = 12 %);
- Nickel wires (90 μm);
- Stainless steel wires (330 μm).

The experimental procedure (brief description):

- Metal wires were evenly spaced using *U*-shaped bolt with threaded arms as a template. The distance between pitches in the thread defines the distance between wires;
- The wires were covered with epoxy glue;
- The membrane was attached to the both sides of the wires (top and bottom);
- The assembly was cured at 80 °C for 1 h.

Assembly modification:

- the assembly was treated with plasma to activate the surface (18 W for 5 min);
- PGMA polymer was deposited on the assembly surface by dip-coating from 1 wt. % solution in methyl ethyl ketone (MEK) and grafted to the membrane and wire surfaces at 120 °C for 1 h;
- residual PGMA was removed by rinsing and washing in pure MEK for 30 min;
- hydrophobic acids were grafted to the PGMA from vapor at 150 °C for 16 h;
- residual acids were removed by rinsing and washing in pure MEK for 30 min;
- Individual membranes were modified in the same way.

Testing procedure:

- water vapor penetration through the individual membranes and the assembly was measured by weight loss of water in the vial covered with the sample under the test;

- in case of the assembly the top membrane's surface (facing outer environment) was sealed to allow the vapor to escape only on the side of the membrane assembly.

Morphology of individual membrane samples was tested by scanning probe microscopy (SPM) and performed on a Dimension 3100 (Digital Instruments, Inc.) microscope. Tapping mode was used to study surface morphology of membranes in ambient air. Silicon tips with spring constants of 40 N/m (tapping mode) were used. Imaging was done at scan rates of 0.5–1 s⁻¹.

3.3. Gradient Fabric

Gradient fabric preparation procedure:

- Plain weave polyester fabric (Test Fabric Inc.) was treated with 40 wt. % aqueous sodium hydroxide for 2 min to activate the surface;
- The fabric was immersed in a 0.5 wt. % solution of PGMA in MEK and grafted in the solution for 3 h at 50 °C;
- Carboxyl-terminated polystyrene (PS-COOH, Polymer Source Inc., $M_n = 48,000$ Da, PDI = 1.05) was deposited by dip-coating from a 2 % (w/v) solution in toluene;
- The fabric was placed in the oven at 150 °C and gradually withdrawn from it at a rate of 0.5 cm/min, thus establishing a gradient of grafting densities that are correlated to the duration of thermal exposure.
- Residual PS-COOH was removed by washing the fabric in toluene for 2 h;
- Poly(acrylic acid) (PAA, Sigma–Aldrich, $M_w = 100,000$ Da) was deposited by dip-coating from a 1% wt./vol. methanol solution;
- The polymer was grafted at 120 °C for 6 min;
- Residual PAA was removed by washing the fabric in methanol for 2 h;
- Uniformly loaded hydrophilic (PAA) and hydrophobic (PS-COOH) fabrics were prepared using the same procedure (grafted at 130 °C).

Contact angle (CA) measurements were performed with water to evaluate the wettability of individual membranes, the membrane assemblies and the fabrics. The measurements were conducted at room temperature using the sessile drop method; equilibrating time was 30 s. Results were recorded on the drop shape analysis instrument (DSA, Kruss, Germany) with the DSA software.

4. RESULTS AND DISCUSSIONS

4.1. Membrane Assembly

A piece of produced membrane assembly is shown in Figure 4. The shape of the assembly can be changed arbitrarily without any loss of integrity of the assembly (Figure 4, right). The distance between membranes in the assembly is set by the size of wires and can be easily controlled and adjusted by changing the wires' dimensions (Figure 5). Successful modification of the membranes by PGMA anchoring layer was confirmed by atomic force microscopy images (Figure 6).



Figure 4. Sample of the Membrane Assembly: Flat (left) and Bent (right)

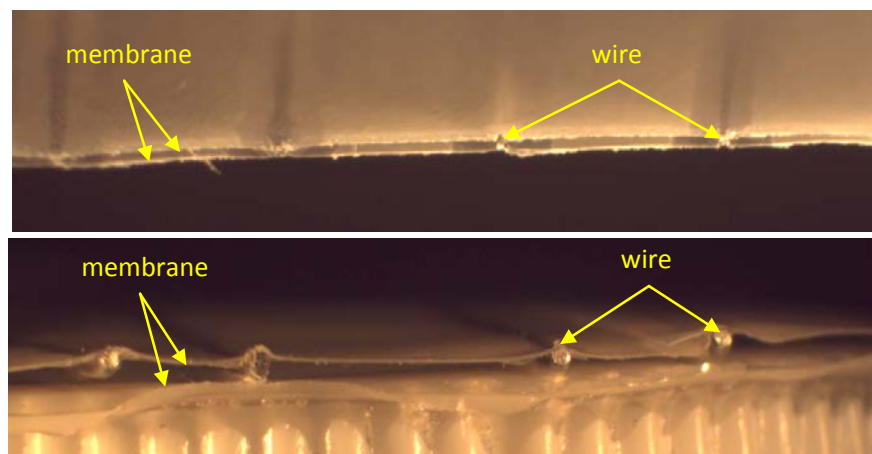


Figure 5. Membrane Assembly Made with 90- μm (top) and 330- μm (bottom) Wires

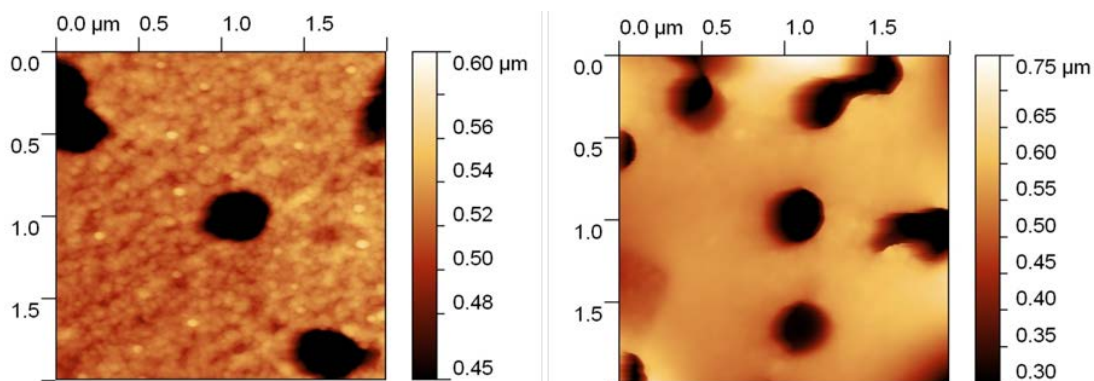


Figure 6. AFM Images of the Membrane: Original (left) and Modified with PGMA (right)

Successful modification of the membrane with a hydrophobic layer was confirmed by CA measurements (Figure 7). This modification of the surface with a hydrophobic layer is essential because it prevents water from wetting the membrane and blocking pores, which might hinder the evaporation process.

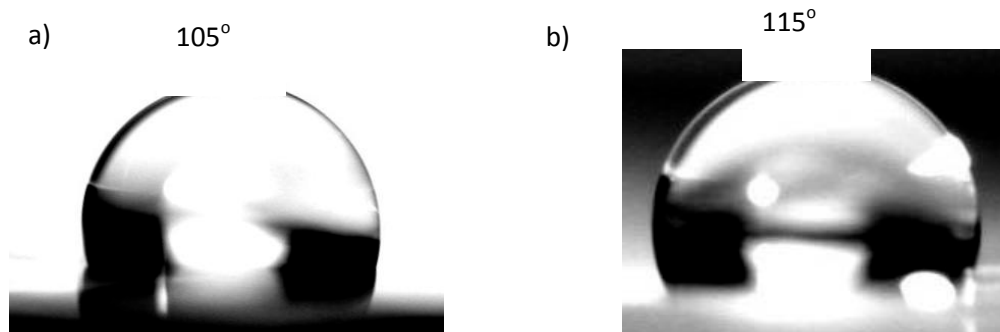


Figure 7. Water Droplets on Membranes Treated with a) Lauric Acid and b) Perfluorododecanoic Acid

Table 1 summarizes all results and experimental conditions used for evaporation studies. For the assemblies at room temperature conditions, significant water condensation was observed (Figure 8, notice the water droplets along the wires, more water was present inside the assembly that is not visible in the picture).

This condensation is a direct consequence of slower water transport through the side of the assemblies than through single-membrane samples, and of the temperature difference between the water and top membrane (the temperatures for S#9 in Table 1 were about the same, which corresponds to the real condition in the space between a body and a vest—and no condensation was observed).

Table 1. Results of Evaporation Tests

S#	$T_{\text{water}}, ^\circ\text{C}$	$T_{\text{outside}}, ^\circ\text{C}$	$\text{RH}_{\text{outside}}, \%$	Sample type	Surface type	Evaporation rate, $\text{mg}\cdot\text{h}^{-1}\text{cm}^{-2}$
1	34 ± 1	24.0 ± 0.5	30 ± 1	single membrane	original	64 ± 1
2					lauric acid	56 ± 1
3					perfluoro-dodecanoic acid	55 ± 1
4	40.0 ± 0.5	23.5 ± 0.5	34 ± 1	open surface	-	64 ± 2
5		23.0 ± 0.5	31 ± 1	single membrane	original	77 ± 3
6	40.0 ± 0.5	23.0 ± 0.5	29 ± 1	assembly (90- μm wire)	original	24 ± 2
7					lauric acid	20 ± 1
8	40.0 ± 0.5	22.0 ± 0.5	21 ± 1	assembly (330- μm wire)	lauric acid	23 ± 1
9						40.5 ± 0.5



Figure 8. Water Condensation inside the Membrane Assembly

4.2. Surface Differential Scanning Calorimeter (SDSC)

The key element behind reliable operation of the SDSC is consistent performance of the two systems under equivalent conditions (reference and sample systems are identical). Several experiments were performed to verify such performance. In general, the two systems differed by ~ 0.01 W and ~ 0.2 °C when operated in constant temperature and constant power modes, respectively. Furthermore, the systems demonstrated identical performance in constant-temperature mode when set at several temperature values (Figure 9). The results demonstrate very good reliability of the SDSC.

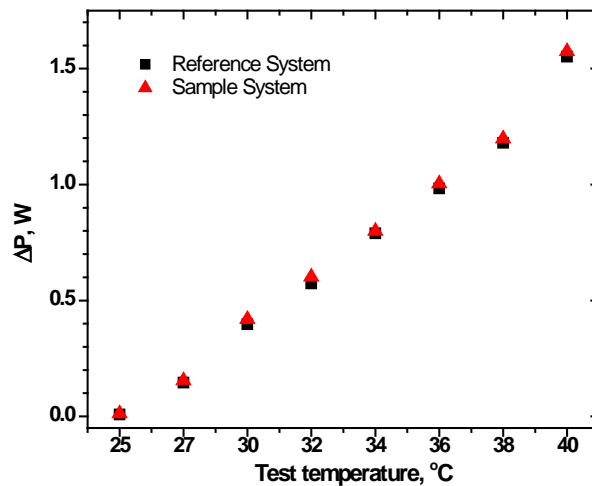


Figure 9. Power Supplied to Identical Reference and Sample Systems at Different Set Temperatures

Reproducibility of the experimental results was checked by performing a few experiments under identical environmental conditions and set-up arrangements. The results obtained for the two systems were found to agree within experimental error. This again indicates very good repeatability and reproducibility of the SDSC.

4.3. Initial Experiments

4.3.1. Single-Membrane and Membrane Assembly

Initial tests with the experimental setup were performed with Styrofoam as a top insulation and one RTD sensor at the center of the heater. Three different arrangements of the sample system were tested:

1. Open, wet fabric (no insulation on top);
2. hydrophilic/hydrophobic membrane on top of the fabric (no insulation on top);
3. hydrophobic membrane assembly with the wire (330 μm) as a spacer (insulated on top)

In all experiments performed the temperature inside the chamber was held constant at 35.5 ± 0.5 $^{\circ}\text{C}$. The results are presented in Figure 10.

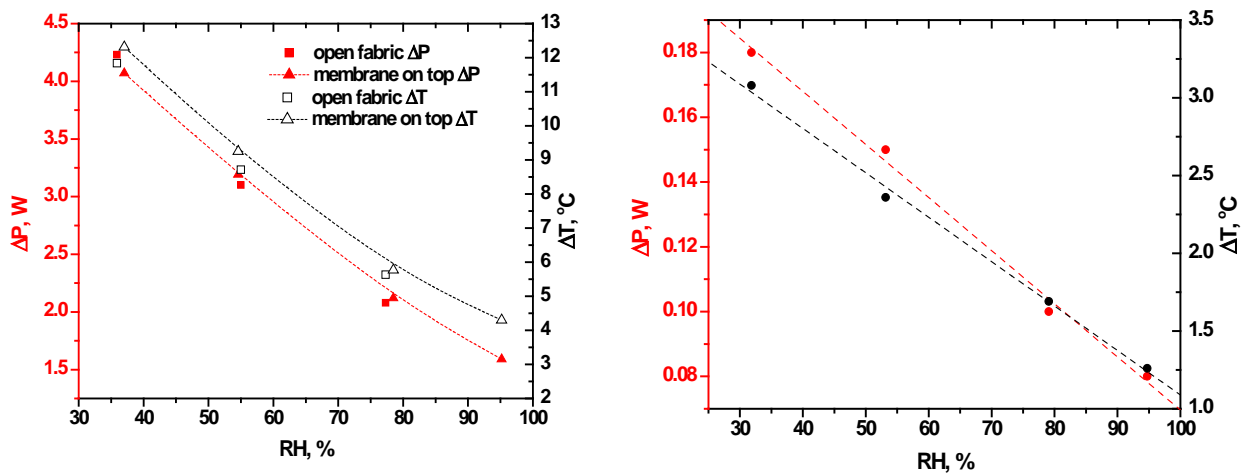


Figure 10. Experimental Results for the Set-up: without Top Insulation with Bare Fabric and the Fabric Covered with the Membrane (left); with Top Insulation and the Membrane Assembly on Top of the Fabric (right)

“Open fabric” configuration lacks any top insulation, simulating the situation without protective clothing. In our experiments this arrangement can generate about 400 Wm^{-2} of cooling power, compensating entirely for the heat generated by a moderate work rate [17] as is achieved naturally through evaporation of water on the skin’s surface.

For the open surface, the resulting average “skin” temperature at moderate humidity was in the vicinity of $31\text{--}32$ $^{\circ}\text{C}$, which is close to the average temperature for human skin [18]. This result shows that the SDSC produces values consistent with those observed in real life.

Hydrophobic and hydrophilic PET membranes show the same results as open bare fabric. These results provided useful in preparation of the modified hydrophobic membrane. Essentially, it prevents direct contact between water in a fabric and any arrangements of materials under the test *without decreasing the evaporation and cooling rates*.

Next, the experimental setup was improved by incorporating four RTD sensors at the center of the assembly and the top of the Styrofoam insulation. This improved the accuracy of temperature

measurements (now averaged over four sensors) and control over temperature fluctuations inside reference and sample systems.

4.3.2. Influence of Air Gap and Water Absorbents

Figure 11 shows the results for evaluation of power and temperature differences at different RH values (temperature inside the chamber = 35.5 ± 0.5 °C).

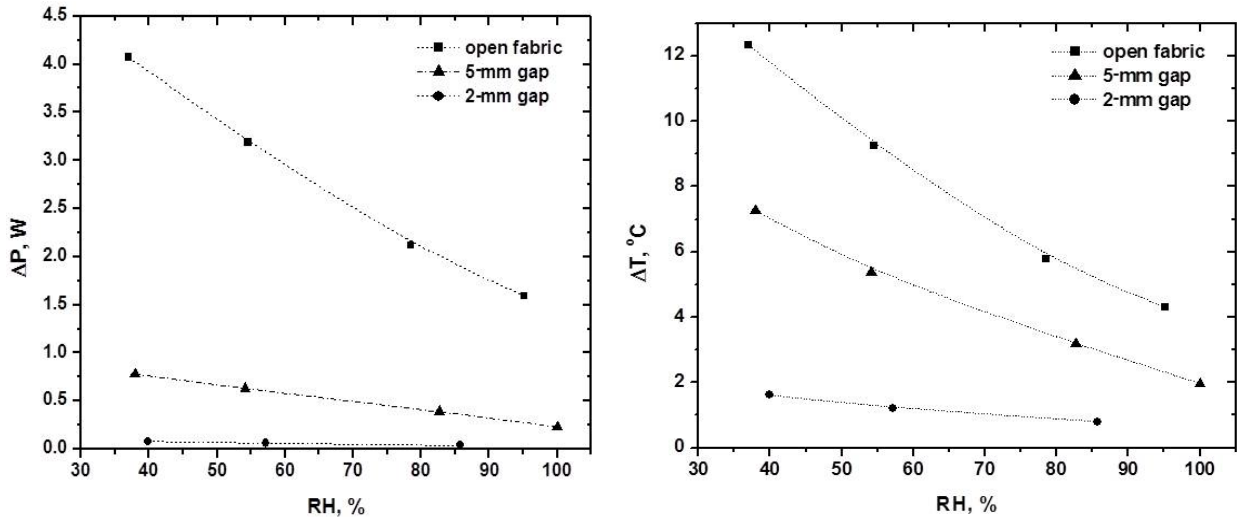


Figure 11. Experimental Results for Power (left) and Temperature Difference (right) for Various Size of Air Gap between the Fabric and the Top Insulation

For both 2- and 5-mm air gaps, water condensed on the insulation surface above the fabric (Figure 12). The temperature of the top insulation surface facing the fabric was found to be only 0.3–0.5 °C lower than the fabric itself. Considering condensate is formed at 100 % RH, RH in the gap space close to the fabric was estimated to be near 98 %. Table 2 presents results from additional experiments performed to eliminate the condensate and study the influence of moisture absorbents on cooling performance of the system ($T = 35.5 \pm 0.5$ °C, 35–40 % RH).

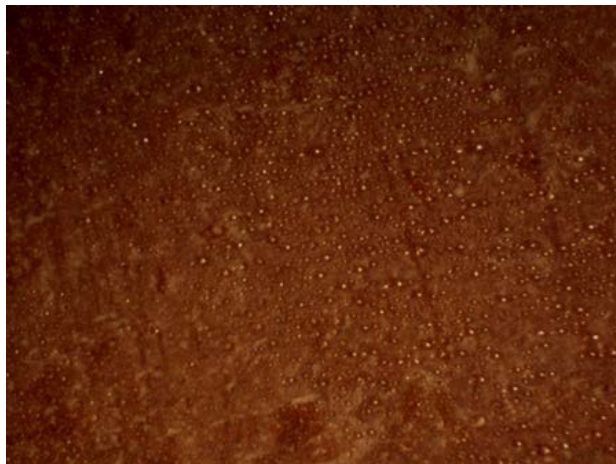


Figure 12. Water Condensed on the Top Insulation's Surface Facing the Fabric

Table 2. Results of the Experiments Aimed to Eliminate the Condensate

Material Tested	Conditions	ΔT (°C)
Membrane Assembly	-	1.4
	4 g Silica gel	2.1
	Filter paper pocket (no absorbent)	2.0
	2 g Silica gel (150-Å pore size) + 2 g sodium polyacrylate (SPA) in filter paper pocket	2.7
Bare Fabric	2-mm air gap	1.6
	2-mm gap (1 mm air + 1 mm metal mesh) + filter paper pocket	2.1
	2-mm gap (1 mm air + 1 mm metal mesh) + 2 g silica gel (60 Å) + 2 g SPA in filter paper pocket	3.5
	3-mm gap (2 mm air + 1 mm metal mesh) + 2 g silica gel (60 Å) + 2 g SPA in filter paper pocket	4.1
	3-mm air gap (2 mm air + 1 mm metal mesh) + filter paper pocket	2.7

It is evident that the introduction of a water absorbent such as a simple layer of filter paper improved the temperature difference by an additional 0.5 °C. More-absorbent materials, such as sodium polyacrylate (SPA) or silica gel, when present alone, did not improve the performance significantly (0.7–0.8 °C). Silica gel saturated very fast in RH near 100 %. The layer of SPA closest to the fabric saturated first and swelled, blocking vapor access to the remaining volume of the polymer. At the same time, a mixture of silica gel and SPA provided a performance boost of 1.5–2 °C compared to the system without any absorbents. The experiments demonstrated that eliminating the condensate improved the cooling performance.

4.4. Gradient Fabric

We performed pilot experiments on preparation of pure PAA-, polystyrene (PS)- and PGMA-modified fabrics. That the fabrics were modified successfully is evidenced by CAs displayed in Figure 13. On a flat surface CAs for PGMA and PS were about 70° and 90°, respectively, and the PAA surface showed a small CA due to its extreme hydrophilicity. The larger CAs seen for PS and PGMA, and complete wetting of PAA were caused by surface roughness of the fabric.

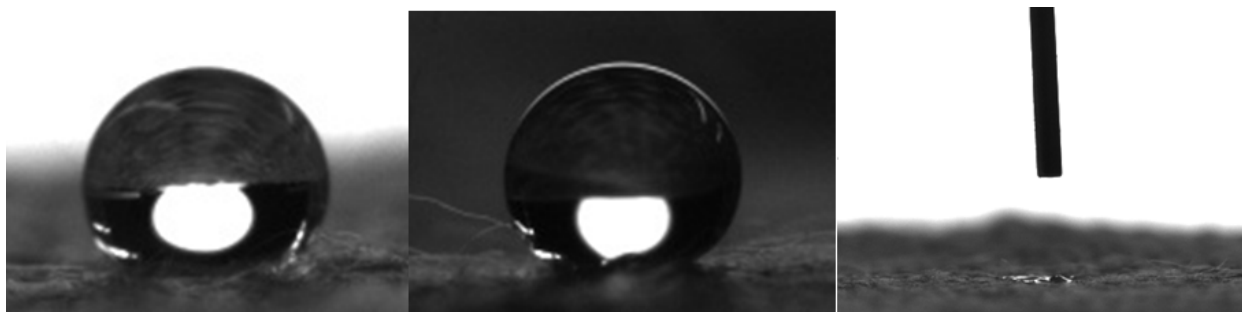
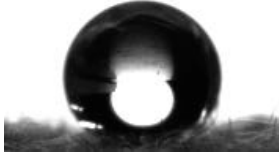
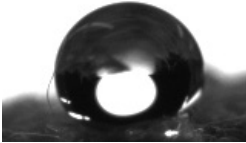





Figure 13. Water Droplets and Contact Angles on Fabrics Modified with PGMA (130° (left); PS-COOH (140°) (middle) and PAA (Completely Wetted) (right)

Next, a gradient fabric was prepared. Table 3 presents CA values measured along the length of the fabric. In initial experiments on the gradient fabric preparation a monotonic gradient was created (from completely hydrophobic on one end to completely hydrophilic on another end). For actual testing of the cooling arrangements a bidirectional gradient fabric was prepared (completely hydrophobic at the center to completely hydrophilic on the sides).

Table 3. Contact Angle Values Along the Gradient Fabric Length

Distance from edge of fabric, cm	Contact Angle, °	Optical Image of Water Drop on Fabric Surface
0–2	143	
2–4	133	
6–8	90	
8–10	54	
10–12	0	

4.5. Cooling Systems

4.5.1. Small Samples (10 cm × 10 cm)

As we demonstrated in Section 4.3.2., a simple air gap can produce a sizable cooling effect. To enhance this effect, a gradient- and a pure-polymer-modified fabric were attached to the top insulation. The obtained results are presented in Figure 14 (conditions: $T = 35.5\text{ °C}$, 55 % RH, air gap = 3 mm), and the gradient fabric achieved a better result than did the completely hydrophilic or completely hydrophobic fabrics.

The significant cooling effect (for the 5-mm gap in particular) probably originates in the diffusion of cooler outside air into the inside space and cooling of the top insulation. The lower temperature of the top insulation facilitates condensation of water vapors (Figure 12), from which effective evaporation can produce a sizable cooling effect. The observation of cooling of the surface of the top insulation and the attendant cooling effect inspired the creation of new cooling system design (Figure 15).

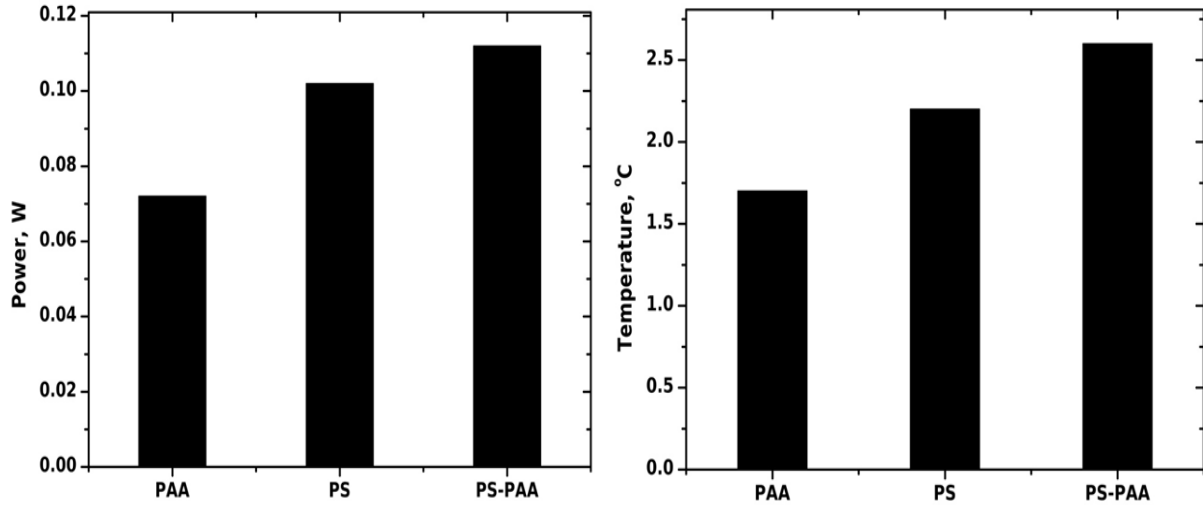


Figure 14. Cooling Power (left) and Temperature Effect (right) Measured with Polymer-Modified Fabrics

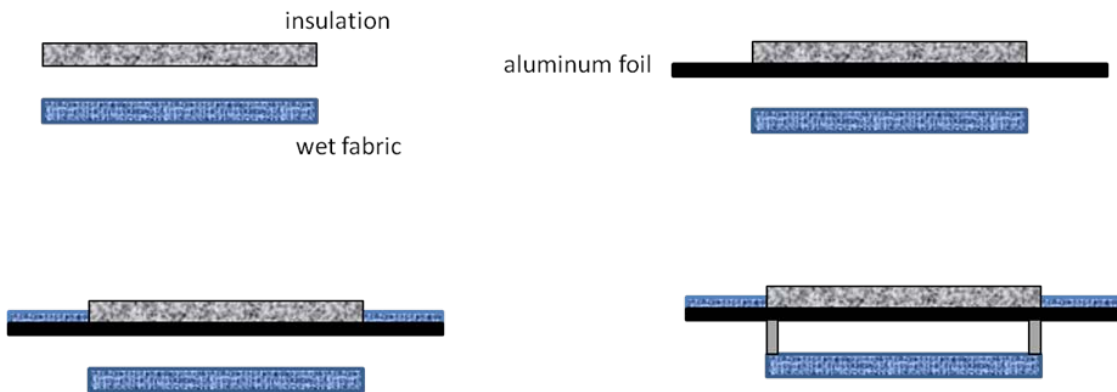


Figure 15. Schematic Representation of Cooling Systems: Standard (top left); with Bare Metal Foil at the Top (top right); with the Foil Covered with Wet Fabric at the Top (bottom left); and System III Isolated from the Outside Environment (bottom right)

Due to its high thermal conductivity the metal foil can transport heat from the inside to the outside fast. Thus, a greater cooling effect can be produced (Figure 16 (conditions: $T = 35.5\text{ }^{\circ}\text{C}$, 55 % RH, air gap = 3 mm)). About four times more cooling power can be achieved just by using aluminum foil. The cooling power can be increased by decreasing the temperature of the portion of foil located outside. To promote cooling, the foil portion located outside was covered with wet fabric.

Figure 17 compares results obtained for four cooling arrangements (conditions: $T = 25\text{ }^{\circ}\text{C}$, 40 % RH, air gap = 3 mm). Notable were the increased cooling power of System III ($\sim 45\text{ Wm}^{-2}$) and the minimal change in power when it was isolated from the outside environment. The last fact indicates that the system is not strongly dependent on environmental conditions and so can be designed as a closed system.

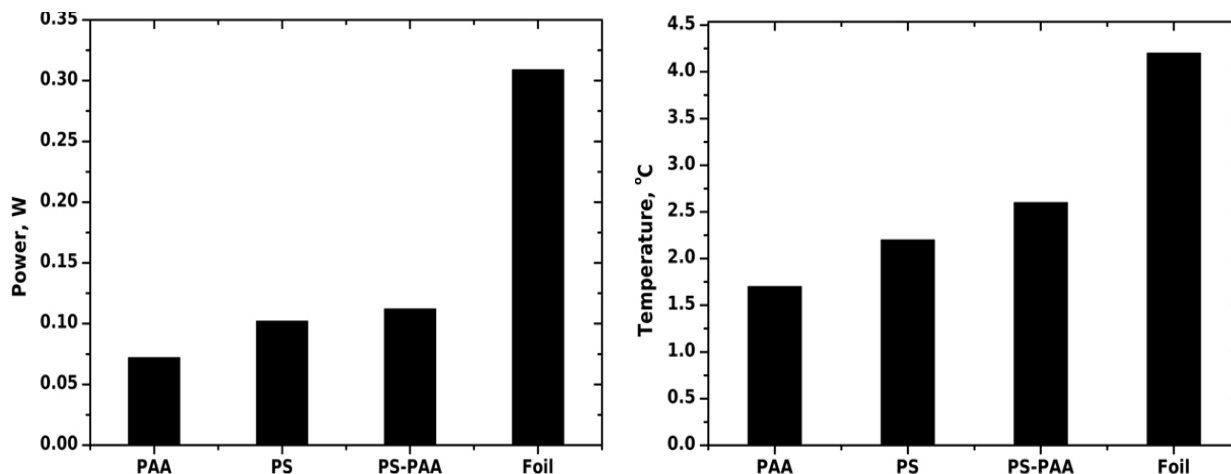


Figure 16. Cooling Power (left) and Temperature Effect (right) of the Standard Cooling Arrangement (System I) with Modified Fabrics and System II (Aluminum Foil)

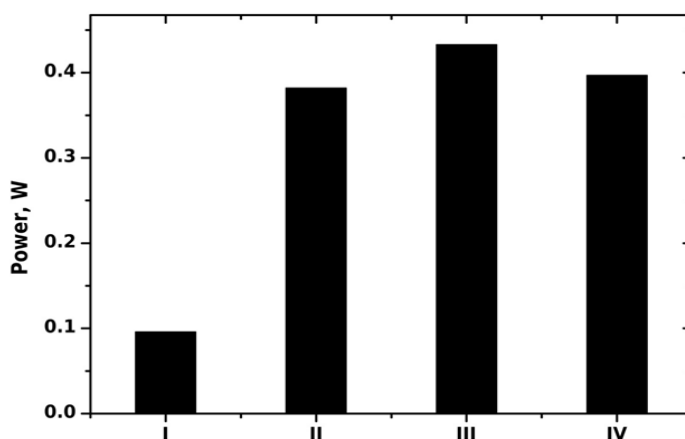


Figure 17. Cooling Power Measured for Cooling System Arrangements I–IV

Further experiments were performed in the chamber, in which bare foil located on the outside was in equilibrium with the environment and held an average temperature of about 35 °C. It was found that evaporation of water at 35 °C can lower the temperature of the foil to 30 °C. Thus, the temperature can be decreased significantly without any external power requirements through a natural evaporative cooling process.

In addition to measuring the actual cooling effect in the environment of the chamber, we tested the influence of gradient and PAA fabrics on the system’s performance (Figure 18) (conditions: $T = 34$ °C, 40 % RH, air gap = 3 mm). The initial short period of rapidly decreasing power corresponds to establishing equilibrium in the system. The window of constant power comprising the second period characterizes the steady-state conditions for wet fabric on the foil (the cooling effect for System III), and the subsequent trend of gradually decreasing power reveals the eventual depletion of water in the fabric. The constant value of power reached after the second decline is that of the dry fabric (true cooling effect for System II).

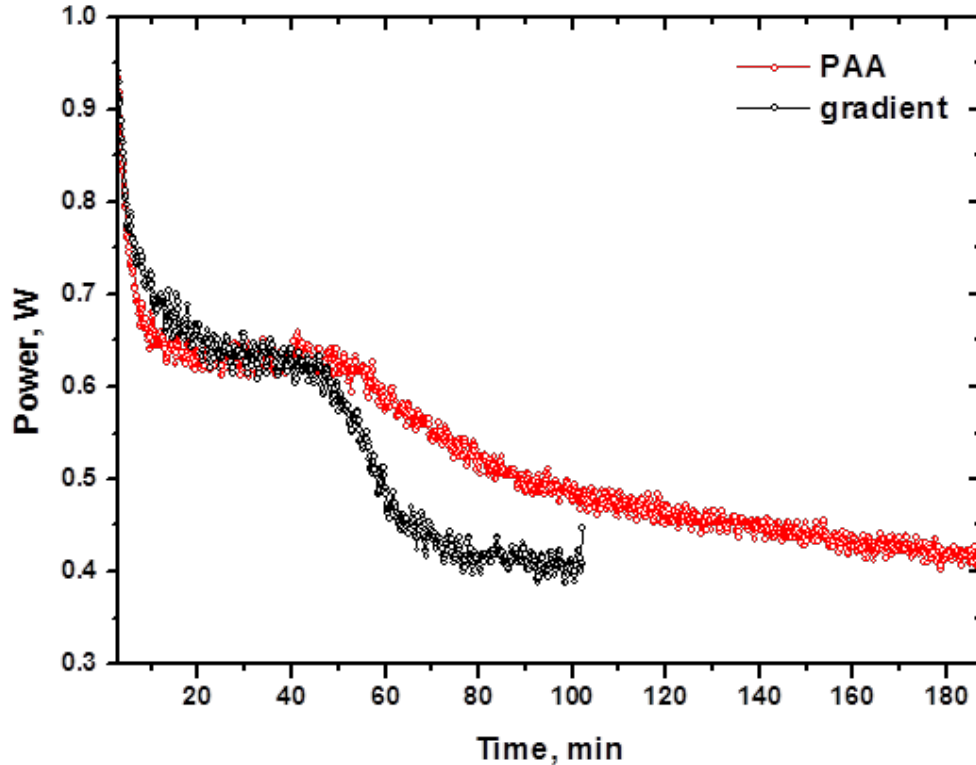


Figure 18. Cooling Power for System III in Presence of Gradient and PAA Fabrics

As shown in Figure 18, the cooling power of System III reached about 65 Wm^{-2} and for System II the same 40 Wm^{-2} was observed as was determined previously (60 % increase compared to System II and more than 600 % increase compared to the original System I). The gradient fabric showed the same performance as the PAA fabric.

To boost the performance of the system further we inserted another copper foil in the space between the heater and the wet fabric simulating the skin (System V, Figure 19 (top)). By this means we introduced an additional route of transporting the heat away from the body. In a real-life situation a copper mesh, not a foil, can be positioned in close proximity to the skin. The porous mesh allows water transport to the surface and evaporation. As a matter of convenience we used copper foil. The result obtained is presented in Figure 19 (bottom).

Several regions merit notice in Figure 19 (bottom). The three plateaus correspond to steady states: I, both fabrics (top and bottom) on the foil are wet; II, one of the fabrics is wet; and III, both fabrics have dried. The new system provided an additional boost in performance, reaching a new high of about 90 Wm^{-2} (and local cooling power values of 100 Wm^{-2} were seen). Even dry foils achieved a useful value, $\sim 60 \text{ Wm}^{-2}$. An additional characteristic of the systems with metal foils is that they can produce constant cooling power for a very long time despite heavy condensation of water on the top foil. The system presented in Figure 19 performed at 60 Wm^{-2} power for almost 24 h, when the experiment was arbitrarily stopped.

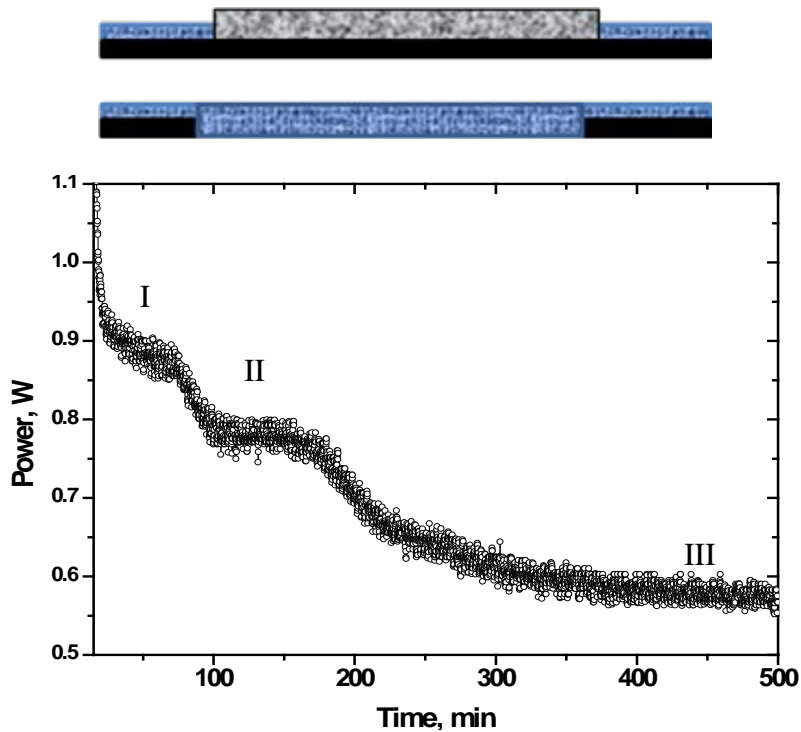


Figure 19. Improved Cooling Arrangement—System V (top) and Cooling Power Produced by System V (bottom)

4.5.2. Large Samples (20-cm × 20-cm)

To estimate the performance of the cooling system integrated in a real-life armor vest, measurements were performed using a larger (20-cm × 20-cm) heater, whose surface area was four times larger than the initial 10-cm × 10-cm heater. The larger dimensions made it impossible to fit the two-system (control and sample) setup into the limited space inside the chamber. Instead, we first carried out the experiment using one heater completely isolated (no evaporation) and with no cooling arrangement to estimate the equilibrium power required to keep the system temperature at 40 °C. Then, the cooling arrangement was added, transforming the unit into the sample system. The power value obtained from the first experiment was used to calculate cooling power in constant-temperature mode and as the power input in constant-power mode.

The external surface area of the copper foils was the same for both the small and larger heater. The equilibrium power value determined for the non-evaporative (reference) system was about 0.44 W, in excellent agreement with the value observed for the smaller heater (0.10 ~ 0.11 W) recalculated for the 4x larger surface area.

We used System V in the cooling experiments. The results are plotted in Figure 20. As shown the total cooling power for the larger system is $2.94 - 0.44 = 2.5 \text{ W}/0.04 \text{ m}^2$ or about 63 Wm^{-2} . This result is very good, but somewhat less impressive than that of the smaller system. The main reasons for this difference are that, compared to the small system, the distance from the center of the heater and RTD elements to the edges of the copper foil is greater but the area of copper exposed outside the large system is not. As a result heat transport is less efficient. We foresee that the cooling power can be improved by using a copper foil of larger area.

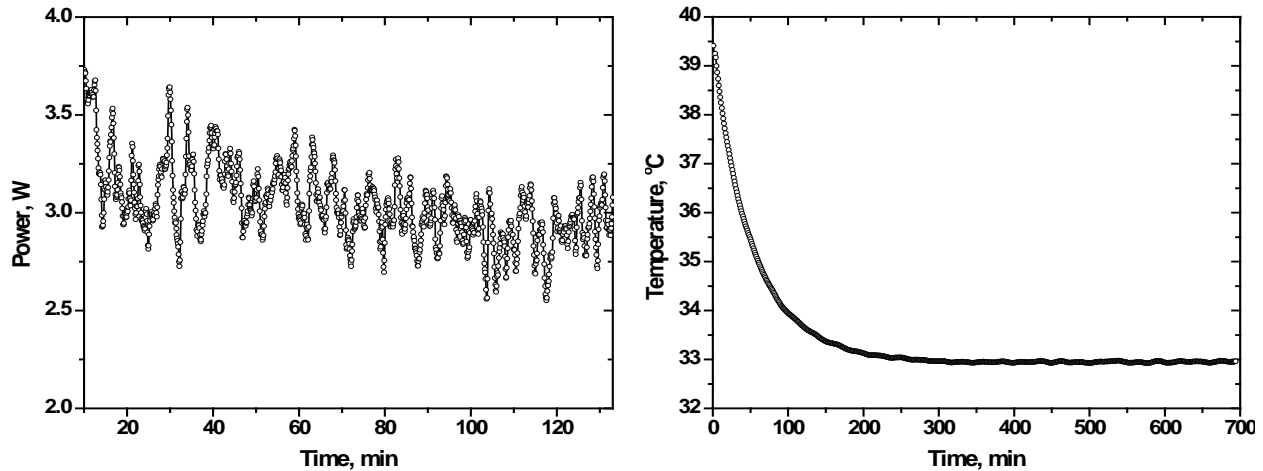


Figure 20. Cooling Power (left) and Temperature Effect (right) of System V Using the Larger Heater

The observed temperature effect is excellent (Figure 20 (right)). In essence, it provides a drop of 7 °C—to near the normal skin temperature of a subject not wearing an armor vest.

4.6. Ultimate Design of the Cooling System

The ultimate design is based on System V and is depicted in Figure 21. Sweat from the body is transferred to the outside by the gradient fabric 5, transporting water from hydrophobic to hydrophilic regions. Water so transferred evaporates from the outer surface of the fabric. Evaporation cools the foils, triggering water condensation on the inner part of the foil at the armor vest’s surface and creating a humidity gradient inside the gap. This gradient promotes evaporation of water from the body’s surface. Water condensed on gradient fabric 4 is transferred outside by the hydrophobic–hydrophilic gradient. Once outside, this water evaporates, contributing to the total cooling effect exerted on the outside parts of the foil—*water needed for the system’s operation is supplied by the system itself*. Several variants of the design are possible (for example, the foil can comprise two separate parts, top and bottom, and cool themselves from separate water supplies).

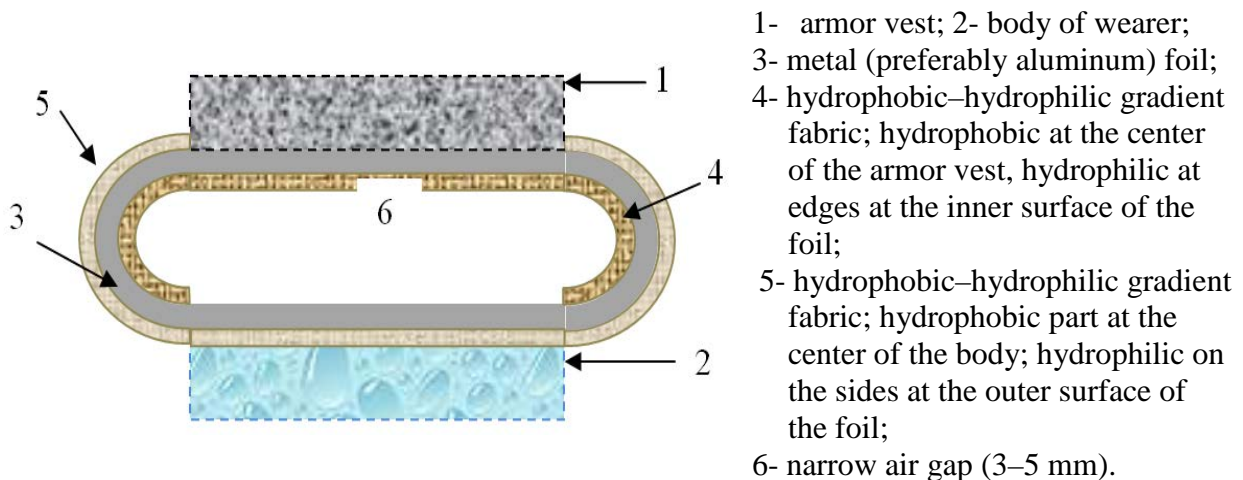


Figure 21. Schematic Representation of the Ultimate Design of the Cooling System

5. CONCLUSIONS

- SDSC was designed and built to measure the cooling power and temperature effect created by various cooling arrangements. The SDSC measures both effects very reliably.
- Methodology was developed to prepare hydrophobic membranes and a flexible membrane assembly, which prevent direct contact of sweat with the components of the cooling system and provide an unobtrusive pathway for water evaporation.
- Methodology was developed to prepare an extraordinarily large-gradient fabric to allow directional water transport within the cooling system. System performance using the gradient fabric was superior to that seen for fabrics with uniform wettability.
- Several cooling systems based on a simple air gap were tested; some incorporated water absorbents. Such systems demonstrated a moderate cooling effect—average temperature decrease of ~ 3 °C.
- A novel cooling system arrangement utilizing the high thermal conductivity of a metal foil was introduced and tested. Several system designs were studied.
- System V, which incorporates self-cooling metal “wings,” performed best. It uses no external power to operate, is lightweight and was able to produce $\sim 100 \text{ Wm}^{-2}$ of cooling power for $10\text{-cm} \times 10\text{-cm}$ samples and $\sim 65 \text{ Wm}^{-2}$ for fourfold larger samples.
- The system is capable of producing a temperature drop $7\text{--}8$ °C and keeping the temperature of the surface close to a normal skin temperature.
- The design is lightweight, compact, self sufficient and can be made as a closed system, isolated from the outside environment.
- An ultimate design was proposed for the cooling system.

6. REFERENCES

1. Gibson, P. W.; Factors influencing steady-state heat and water vapor transfer measurements for clothing materials; *Textile Research Journal* 1993, 63, 749-764.
2. Nunneley, S. A.; Heat stress in protective clothing: Interactions among physical and physiological factors; *Scandinavian Journal Of Work, Environment And Health* 1989, 15, 52-57.
3. Cadarette, B. S., DeCristofano, B. S., Speckman, K. L., et al.; Evaluation of three commercial microclimate cooling systems; *Aviat Space Environ Med* 1990, 61, 71-76.
4. Reffeltrath, P. A.; Heat stress reduction of helicopter crew wearing a ventilated vest; *Aviation Space and Environmental Medicine* 2006, 77, 545-550.
5. Lehmacher, E. J., Jansing, P., and Küpper, T.; Thermophysiological responses caused by ballistic bullet-proof vests.; *The Annals of occupational hygiene* 2007, 51, 91-96.
6. Chevront, S. N., Goodman, D. A., Kenefick, R. W., et al.; Impact of a protective vest and spacer garment on exercise-heat strain; *Eur J Appl Physiol* 2008, 102, 577-583.
7. Hadid, A., Yanovich, R., Erlich, T., et al.; Effect of a personal ambient ventilation system on physiological strain during heat stress wearing a ballistic vest; *Eur J Appl Physiol* 2008, 104, 311-319.
8. Lee, K. C., Tai, H. C., and Chen, H. C.; Comfortability of the bulletproof vest: Quantitative analysis by heart rate variability; *Fibres Text. East. Eur.* 2008, 16, 39-43.
9. Barwood, M. J., Newton, P. S., and Tipton, M. J.; Ventilated vest and tolerance for intermittent exercise in hot, dry conditions with military clothing; *Aviat Space Environ Med* 2009, 80, 353-359.
10. Cao, H., Branson, D. H., Peksoz, S., et al.; Fabric selection for a liquid cooling garment; *Textile Research Journal* 2006, 76, 587-595.
11. Bogerd, N., Psikuta, A., Daanen, H. A. M., et al.; How to measure thermal effects of personal cooling systems: Human, thermal manikin and human simulator study; *Physiol Meas* 31, 1161-1168.
12. Bendkowska, W., Klonowska, M., Kopias, K., et al.; Thermal manikin evaluation of pcm cooling vests; *Fibres Text. East. Eur.* 18, 70-74.
13. O'Brien, C., Blanchard, L. a., Cadarette, B. S., et al.; Methods of evaluating protective clothing relative to heat and cold stress: Thermal manikin, biomedical modeling, and human testing; *Journal of occupational and environmental hygiene* 8, 588-599.
14. Xu, X., Endrusick, T., Laprise, B., et al.; Efficiency of liquid cooling garments: Prediction and manikin measurement; *Aviat Space Environ Med* 2006, 77, 644-648.
15. Holmes, D. A.; Waterproof breathable fabrics; *Handbook of technical textiles* 2004, 282-316.
16. Israelski, E. W.; Basic human abilities; *Handbook of Human Factors in Medical Device Design* 2011, 23-63.
17. Holmes, D.A., Waterproof breathable fabrics. In *Handbook of Technical Textiles*; Horrocks, A.R, Anand, S.C, Eds., CRC Press: Boca Raton, 2004; p.283.

18. Israelski, E.W., Basic human abilities. In *Handbook of Human Factors in Medical Device Design*; Weigner, M.B., Wiklund, M.E., Gardner–Bonneau, D.J. Eds., CRC Press: Boca Raton, 2011; p.45.

LIST OF SYMBOLS, ABBREVIATIONS, AND ACRONYMS

CA	contact angle
cm	centimeter(s)
DSC	differential scanning calorimetry
h	hour(s)
MEK	methyl ethyl ketone
min	minute(s)
M_n	number average molecular weight
M_w	weight average molecular weight
PAA	polyacrylic acid
PDI	polydispersity index
PGMA	poly(glycidyl methacrylate)
PI	proportional integral
PS	polystyrene
PS-COOH	carboxyl-terminated polystyrene
PS-PAA	polystyrene–polyacrylic acid gradient
RTD	resistance temperature detector
s	second(s)
SDSC	surface differential scanning calorimeter
SPA	sodium polyacrylate
SPM	scanning probe microscopy
μm	micrometer
Wm^{-2}	watts per square meter
$^{\circ}\text{C}$	degrees Celsius